"BABEŞ-BOLYAI" UNIVERSITY, CLUJ-NAPOCA
FACULTY OF CHEMISTRY AND CHEMICAL ENGINEERING

PhD Thesis

Abstract

SMART CORROSION RESISTANT COATINGS

Scientific Advisor
Prof. Dr. Liana-Maria MUREŞAN

PhD Student
Nicoleta COTOLAN

Cluj-Napoca
2015

"BABEŞ-BOLYAI" UNIVERSITY, CLUJ-NAPOCA
FACULTY OF CHEMISTRY AND CHEMICAL ENGINEERING

Nicoleta COTOLAN

SMART CORROSION RESISTANT COATINGS

PhD Thesis

Abstract

Jury:
President:
Prof. Dr. Luminiţa SILAGHI-DUMITRESCU, "Babeş-Bolyai" University, Cluj-Napoca, Romania
Scientific advisor:
Prof. Dr. Liana-Maria MUREŞAN, "Babeş-Bolyai" University, Cluj-Napoca, Romania

Reviewers:
Prof. Dr. Ingrid MILOŠEV, "Jožef Stefan" Institute, Ljubljana, Slovenia
Prof. Dr. Zoltán HÓRVÖLGYI, University of Technology and Economics, Budapest, Hungary
Assoc. Prof. Dr. Eng. Graziella TURDEAN, "Babeş-Bolyai" University, Cluj-Napoca, Romania

Thesis defense: **October 30, 2015**

TABLE OF CONTENTS

Acknowledgements..... 6

Introduction..... 8

Part I. Theoretical Considerations..... 10

1. Fundamental aspects of metal corrosion and corrosion protection..... 11

1.1. General introduction..... 11

1.2. Metals passivity..... 15

1.2.1. Generalities..... 15

1.2.2. Pourbaix diagrams..... 16

1.2.3. Polarization curves..... 16

2. Corrosion resistant materials..... 18

2.1. Materials based on Ti and Ti alloys..... 18

2.1.1. Generalities..... 18

2.1.2. Materials for medical implants based on Ti..... 19

2.1.2.1. Ti–6Al–4V..... 21

2.1.2.2. Ti–6Al–7Nb..... 21

2.2. Materials based on Zn..... 22

2.2.1. Generalities..... 22

2.2.2. Galvanized steel..... 23

2.3. Preparation methods of corrosion resistant coatings on metals..... 25

2.3.1. Sol-gel method..... 25

2.3.2. Electrochemical oxidation..... 27

3. Investigation methods..... 28

3.1. Electrochemical methods..... 28

3.1.1. Linear polarization..... 28

3.1.2. Potentiodynamic polarization. Tafel representations..... 29

3.1.3. Electrochemical impedance spectroscopy..... 31

3.2. Physico-chemical methods..... 35

3.2.1. Scanning electron microscopy. Energy dispersive X-ray spectroscopy..... 35

3.2.2. High-resolution transmission electron microscopy..... 36

3.2.3. X-ray diffraction……..……. 37
3.2.4. UV-Vis spectroscopy…… 38
Part II. Original Contributions…….…… 41
4. Corrosion resistant coatings on Ti-6Al-7Nb and Ti ……..……. 42
4.1. Aims of the study……. 42
4.2. TiO_2 coatings deposited on Ti–6Al–7Nb by anodic oxidation in sulfuric acid or acetic acid…….……..……..…... 42
4.2.1. Introduction…….. 42
4.2.2. Experimental conditions…….. 44
4.2.2.1. Materials…….…… 44
4.2.2.2. Apparatus and methods……. 44
4.2.3. Results and discussion……...…... 46
4.2.3.1. Determination of oxidation potentials…….…….... 46
4.2.3.2. Anodic oxidation of Ti–6Al–7Nb..……..…… 47
4.2.3.3. Morpho-structural study by SEM-EDS of surfaces……. 48
4.2.3.4. X-ray diffraction analysis…….…. 51
4.2.3.5. Electrochemical corrosion tests…….…. 53
4.2.3.5.1. Open circuit potential..... 53
4.2.3.5.2. Cyclic polarization……..…… 54
4.2.3.5.3. Electrochemical impedance spectroscopy…….…… 56
4.2.4. Conclusions……... 59
4.3. Ag-TiO_2 composite layer with improved corrosion and antimicrobial properties deposited on Ti by sol-gel method…….……...……...……..... 60
4.3.1. Introduction…….. 60
4.3.2. Experimental conditions……... 62
4.3.2.1. Materials……. 62
4.3.2.2. Apparatus and methods……..... 63
4.3.3. Results and discussion…….. 66
4.3.3.1. Phase composition, microstructure, optical properties and morphology of the coatings…….……...…... 66
4.3.3.2. Electrochemical characteristics of the coatings……..... 70

4.3.3.2.1. Polarization resistance and potentiodynamic curves……. 70
4.3.3.2.2. Electrochemical impedance spectroscopy……..……... 73
4.3.3.3. Topography of the coatings……...…. 79
4.3.3.4. Adhesion of bacteria to the coatings…….…… 80
4.3.4. Conclusions…….…… 83
5. Corrosion resistant coatings for galvanized steel…….. 84
5.1. Aim of study…… 86
5.2. Experimental conditions…… 87
5.2.1. Materials……... 87
5.2.2. Synthesis of precursor sols…….….. 88
5.2.3. Preparation of coatings…… 89
5.2.4. Silylation of coatings……..... 91
5.2.5. Incorporation of BTA in the coatings…….. 91
5.2.6. Electrochemical measurements……..... 91
5.3. Results and discussions……... 92
5.3.1. Preliminary measurements on sol-gel coated Zn substrates..……..…… 92
5.3.1.1. Electrochemical measurements……..…… 92
5.3.1.1.1. Polarization curves……. 92
5.3.1.1.2. Electrochemical impedance spectroscopy…….…… 97
5.3.2. Silica coatings on galvanized steel…….……..…… 101
5.3.2.1. Characterization of the samples by SEM measurements…….....**.....** 101
5.3.2.2. HRTEM analysis of the pore structure…….**.....** 102
5.3.2.3. Electrochemical measurements……..…... 103
5.3.2.3.1. Polarization curves……. 103
5.3.2.3.2. Electrochemical impedance spectroscopy…….**....** 110
5.4. Conclusions…….…… 120
General Conclusions…….…… 122
Scientific Activity……..... 124
Papers……..…. 124
Conferences participation…….……..…. 125
References……..……... 126

ACKNOWLEDGEMENTS

Foremost, I would like to express my sincere gratitude to my scientific coordinator **Prof. Dr. Liana-Maria MUREŞAN** for the continuous support of my PhD study and research, for her patience, motivation, enthusiasm and immense knowledge. Her guidance, attention and commitment made possible to finish my research that is summarized in this dissertation and in all the published articles. I could not have imagined having a better advisor and mentor.

Besides my advisor, I wish to express thanks for their acceptance like members of the jury to: **Prof. Dr. Ingrid MILOŠEV**, **Prof. Dr. Zoltán HÓRVÖLGYI** and **Assoc. Prof. Dr. Eng. Graziella Liana TURDEAN**. I also thank them for their valuable guidance, insightful comment and encouragement extended to me which served to improve this thesis. Moreover, many thanks to **Prof. Dr. Ingrid MILOŠEV** and **Prof. Dr. Zoltán HÓRVÖLGYI** for accepting me in their group and for being such good advisors during my stays abroad.

Thanks to **Prof. Dr. Ionel Cătălin Popescu**, **Prof. Dr. Eng. Petru Ilea** and **Assist. Prof. Dr. Eng. Adrian Nicoară** for their help, constructive discussions and valuable suggestion.

I wish to thank to the financial support from the Erasmus Program and the National Development Agency (Hu-Ro Bilateral Co-operation, SOLGELCOR, 664/2013).

Thanks to S.C. BETAK S.A. Bistriţa for supplying the galvanized zinc substrates used in this study.

This PhD thesis work was possible with the financial support from the Sectoral Operational Program for Human Resources Development 2007-2013, co-financed by the European Social Fund, under the project number POSDRU/159/1.5/S/137750 with the title „Doctoral and Postdoctoral Programs - support for increasing the competitiveness of exact sciences research".

INTRODUCTION

The corrosion of metals is a complex process and its effects are very important, being a phenomenon that caused many damages. This phenomenon consists in the partial or whole destruction of metals, caused by chemical, electrochemical or biochemical reactions that are produced between the metal and external factors. Standard metals and alloys, which have been used for many years, are likely to continue to be used into the future unless they contain elements that are targeted for replacement such as chromium.

In the past 20 years titanium and its alloys have gained more and more attraction as materials used for surgical applications because of their prominent mechanical, chemical, and biocompatible properties [1] and it has been well established that titanium is biocompatible, inert and immune to corrosion by all body fluids and tissue [2]. Although titanium is a material with corrosion resistance and biocompatibility in contact with living on tissue, favorable biological response is due to the titanium oxide layer that forms spontaneously on the surface of titanium and is mainly amorphous [3, 4]. This oxide layer has a very small thickness, about 2–3 nm, and may cause problems regarding metal ions release when titanium and titanium alloys surface are in contact with body fluids of living organisms over a long period. On the other hand, to allow the osseointegration process, the contact between the metallic implant and the receiving living tissue is made through the oxide layer on the implant surface [5]. Thus, the most important requirement for the long-term success of implants is the stable interface between the biomedical implant and the surrounding tissue [6].

Zinc is a very active metal so that it corrodes quickly in aqueous solutions [7]. Zinc specimens exposed to an unpolluted dry atmosphere were quickly covered with a thin grey layer of ZnO. When the zinc coating is exposed to atmosphere or immersed in an aqueous solution, ZnO is replaced by a white compact corrosion product of zinc hydroxide, $Zn(OH)_2$, which forms the basis for further growth of corrosion products. Upon reaction with CO_2, zinc transforms into white rust, a complex hydrated zinc carbonate/zinc hydroxide as suggested by Odnevall *et al.* [8].

Zinc it is extensively used as a sacrificial protective coating for ferrous metal products (galvanized steel) and also as a material used in metallic structures submitted to outdoor exposure [9]. Electroplated zinc coatings are widely used in the industry for providing cathodic

protection to steel substrates. Therefore, thick zinc coatings are usually required for long-lasting protection.

In this context, a priority of this study was to increase common level of corrosion resistance of titanium, titanium alloys and galvanized steel by developing different corrosion resistant layers on their surfaces.

The main purposes of the study were:

1) preparation of TiO_2 and Ag-TiO_2 coatings on titanium and titanium alloy substrate by sol-gel method (spin-coating) or electrochemical method (anodic oxidation) and the characterization of the coatings in terms of composition, morphology, topography, electrochemical and antibacterial activity;

2) testing of protective coatings based on SiO_2 deposited on zinc and galvanized steel by sol-gel method (dip-coating) in order to increase the corrosion resistance.

The corrosion behavior of metals was investigated by electrochemical methods, morphological and structural analysis.

Keywords: Corrosion, Zinc, Galvanized Steel, Titanium, Titanium Alloy, Titanium Oxide, Silica Layers, Sol-gel Coatings

Part II. Original contributions

4. Corrosion resistant coatings for Ti–6Al–7Nb and Ti

4.2.3.1. Determination of oxidation potentials

In order to determine the optimal potentials for TiO_2 layers preparation on Ti–6Al–7Nb surface, potentiodynamic polarization experiments were carried out before the anodic oxidation step (Figure 4.2). As it can be observed from Figure 4.2, after the Tafel region, two portions with diminished current densities appear on the polarization curves, indicating the passivity of the investigated alloy: one around 0.7 V and a second, more developed, starting from approximately 2.0 V *vs.* $Ag/AgCl,NaCl_{3M}$.

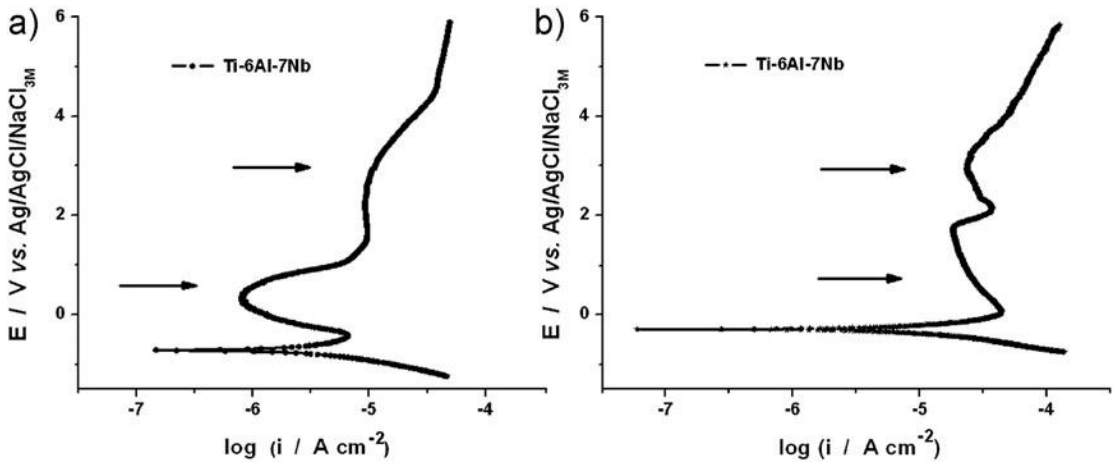

Figure 4.2 Potentiostatic polarization curve obtained for Ti–6Al–7Nb in 1M CH_3COOH (a) and 1M H_2SO_4 (b) using a scan rate of 1 mV s^{-1}. The arrows indicate the selected oxidation potentials.

4.2.3.2. Anodic oxidation of Ti–6Al–7Nb

The current *vs.* time curves measured during potentiostatic oxidation of Ti–6Al–7Nb at 0.7 V and 3.0 V in the two electrolytes are presented in Figure 4.3 in log/log coordinates. As expected, the current density decreases continuously with time.

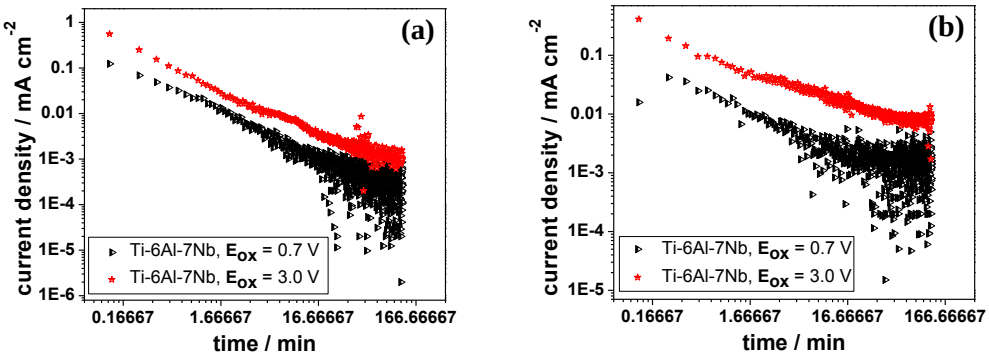

Figure 4.3 Current *vs.* time curves measured during potentiostatic oxidation at 0.7 V and 3.0 V for 120 min in 1M CH_3COOH (a) and 1M H_2SO_4 (b).

4.2.3.3. Morpho-structural study by SEM-EDS of surfaces

Figure 4.4 presents the surface morphology of Ti–6Al–7Nb samples before and after anodic oxidation in CH_3COOH and H_2SO_4.

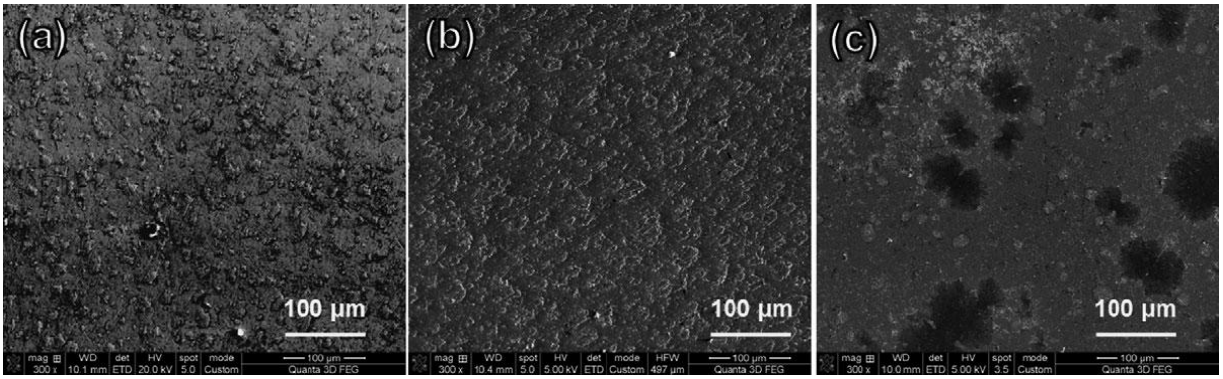

Figure 4.4 SEM micrographs of the unoxidized (a) and oxidized Ti–6Al–7Nb surfaces in CH_3COOH (b) and H_2SO_4 (c)

It can be observed that, after oxidation, the surface became covered with a layer of oxidation products that is more compact and uniform in the case when CH_3COOH was used. The

SEM images show that the film thickness was about 7 µm for TiO_2 obtained in CH_3COOH and around 4 µm for TiO_2 obtained in H_2SO_4 (Figure 4.5).

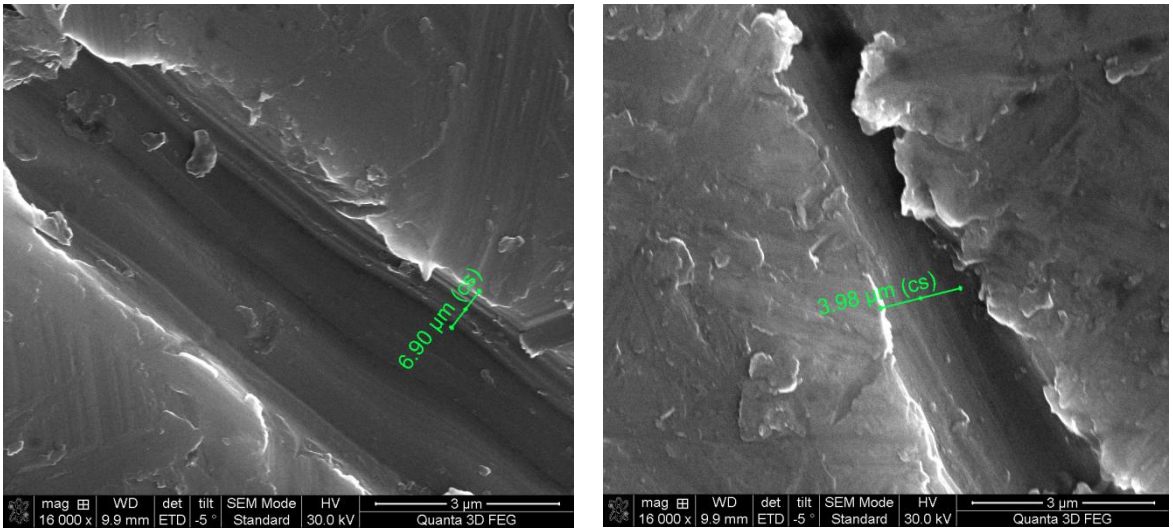

Figure 4.5 SEM images for TiO_2 obtained in acetic acid (left) and for TiO_2 obtained in sulfuric acid (right).

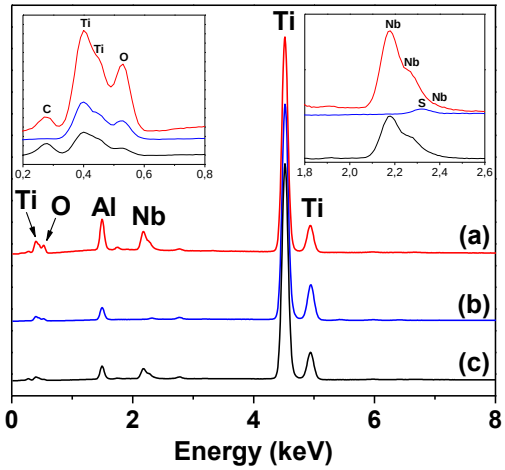

Figure 4.6 EDS spectra of the unoxidized (a) and oxidized Ti–6Al–7Nb surfaces in CH_3COOH (b) and H_2SO_4 (c). The inset contains the EDS spectra in the 0.2–0.8 and 1.8–2.6 regions.

These observations are supported also by the EDS results. The EDS spectra are presented in Figure 4.6, while the percentages of the main components obtained from these spectra are summarized in Table 4.1. The Al and Nb contents estimated by EDS analyses on the unoxidized sample: Al – 5.8 wt% (9.7 at%) and Nb – 6.8 wt% (3.3 at%) are in good agreement with the

percentages reported by the producer for Ti–6Al–7Nb alloy (5.5–6.5 wt% for Al and 6.5–7.5 wt% for Nb, Ti balance).

The EDS spectra (Figure 4.6) evidence the atomic species present in the material and indicate beside titanium, aluminum, niobium, and oxygen the presence of small amounts of residual carbon and sulfur.

The O content increased after oxidation, proving the formation of TiO_2 and was found to have a higher value in the case of the samples oxidized in CH_3COOH (Table 4.1), this result being in good agreement with the XRD results.

Table 4.1 EDS results for unoxidized and oxidized Ti–6Al–7Nb samples. Penetration depth of the electron beam, 33.72 μm for TiO_2 and 5.4 μm for Ti; thickness of TiO_2 film, 4–7 μm.

	Atomic (%)				**Weight (%)**			
	O	**Ti**	**Al**	**Nb**	**O**	**Ti**	**Al**	**Nb**
Unoxidized	7.3 ± 0.4	79.7 ± 0.3	9.7 ± 0.5	3.3 ± 0.7	2.6	84.8	5.8	6.8
Oxidized in H_2SO_4, 3.0 V	16.9 ± 0.7	74.2 ± 0.5	8.9 ± 0.5	–	6.7	87.4	5.9	–
Oxidized in CH_3COOH, 3.0 V	21.0 ± 0.7	66.5 ± 0.7	9.2 ± 0.6	3.3 ± 0.8	8.3	78.1	6.1	7.5

4.2.3.4. X-ray diffraction analysis

In order to get a deeper insight of the anodic oxide layers structure, XRD measurements were carried out. The XRD results of TiO_2 films showed peaks related to the anatase (A) and rutile (R) phases and α–Ti of titanium alloy substrate (Figure 4.7).

For the sample oxidized in H_2SO_4 (Figure 4.7(b)) XRD pattern is determined by the α–Ti peaks attributed to the substrate. The lower intensities peaks of TiO_2 deposit (rutile and anatase phases) suggest that the oxide layer is thin or inhomogeneous. The XRD pattern for the sample oxidized in CH_3COOH (Figure 4.7(a)) shows the more intense peaks corresponding to rutile and anatase phases from TiO_2 layer and only low intensity peaks of the substrate

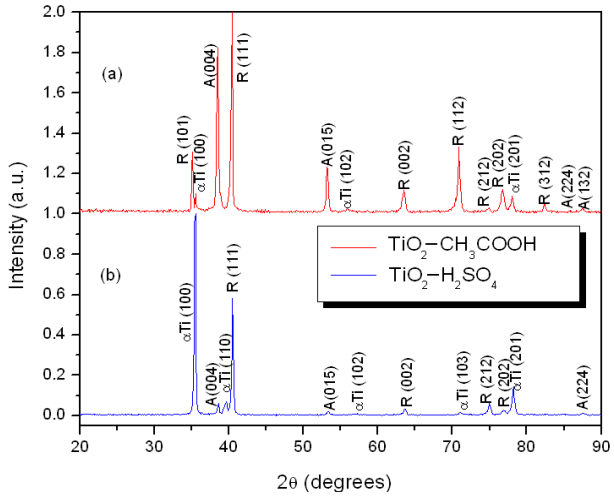

Figure 4.7 XRD patterns of Ti–6Al–7Nb samples oxidized in CH_3COOH (a) and H_2SO_4 (b); A = anatase; R = rutile.

4.2.3.5 Electrochemical corrosion tests

4.2.3.5.2 Cyclic polarization

The cyclic polarization curves for Ti–6Al–7Nb untreated and after anodization in CH_3COOH or H_2SO_4, measured in Hank's solution are presented in Figure 4.8. The switching potential, E_{sw}, was 6.0 V.

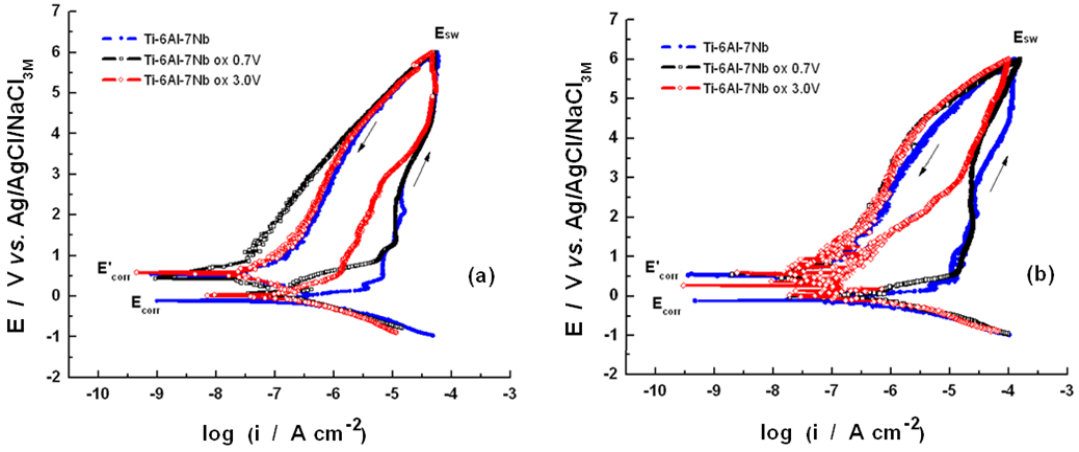

Figure 4.8 Cyclic polarization curves measured in Hank's solution, (pH 7.4, t 37 ºC), for untreated Ti–6Al–7Nb and oxidized in 1M CH_3COOH (a), and in 1M H_2SO_4 (b). Experimental conditions: oxidation potentials, 0.7 V and 3.0 V; oxidation time, 120 min; scan rate, 1 mV s^{-1}; switch potential, E_{sw}, 6.0 V.

The corrosion potential (E_{corr}) and the corrosion current density (i_{corr}) were obtained from the first part of the potentiostatic polarization curves using the Tafel least squares fitting method. The values of the corrosion parameters obtained from polarization curves using Tafel interpretation are shown in Table 4.3.

Table 4.3 Corrosion parameters measured in Hank's solution, for Ti–6Al–7Nb before and after oxidation for 120 min in CH_3COOH or H_2SO_4; $\Delta E = (E_{sw} - E_{corr})$ and $\Delta E' = (E_{sw} - E'_{corr})$.

Sample	E_{corr} (V)	i_{corr} (μA cm^{-2})	E'_{corr} (V)	ΔE (V)	$\Delta E'$ (V)
Untreated Ti–6Al–7Nb	–0.511	0.843 ± 0.001	0.378	6.511	5.622
Ti–6Al–7Nb oxidized at 0.7 V in CH_3COOH	–0.134	0.351 ± 0.003	0.464	6.134	5.536
Ti–6Al–7Nb oxidized at 3.0 V in CH_3COOH	–0.321	0.137 ± 0.004	0.556	6.321	5.444
Ti–6Al–7Nb oxidized at 0.7 V in H_2SO_4	0.298	0.428 ± 0.009	0.570	5.702	5.430
Ti–6Al–7Nb oxidized at 3.0 V in H_2SO_4	0.168	0.077 ± 0.007	0.607	5.832	5.393

4.2.3.5.3. Electrochemical impedance spectroscopy

The corrosion behavior of the untreated and oxidized Ti–6Al–7Nb samples was evaluated by impedance spectroscopy measurements. The experiments were performed after 1 h of immersion in the corrosive solution (pH 7.4, t 37 ºC) to ensure the stability of the system during the impedance measurement.

Figures 4.9 and 4.11 present the impedance spectra for the investigated samples. As it can be easily noticed in Figure 4.9, the visual appearance of the Nyquist plots obtained for samples corrosion in Hank's physiological solution reflects a capacitive behavior. On the other hand, it can be observed that the oxidation induces a significant change of the impedance diagrams in both shape and size. Thus, after AO in either CH_3COOH or H_2SO_4, the impedance modulus increases, due to the formation of a passive layer with barrier properties on the surface.

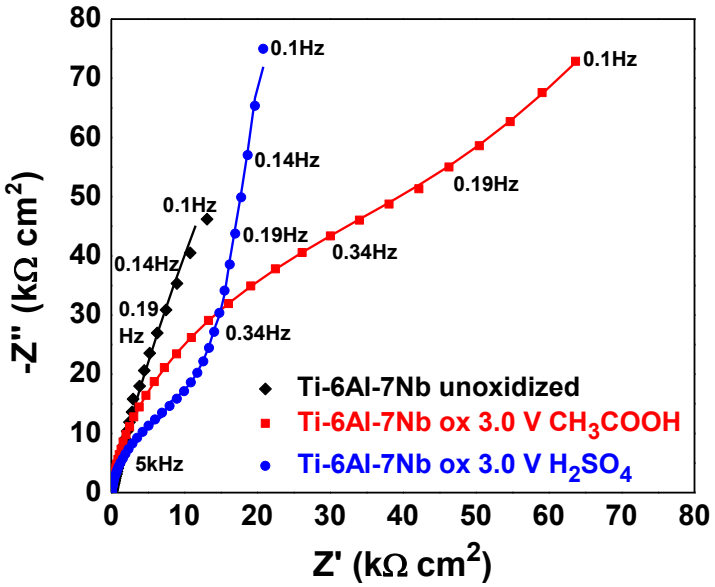

Figure 4.9 Nyquist plots corresponding to the corrosion of untreated and oxidized Ti–6Al–7Nb samples after 1 h immersion in Hank's physiological solution (pH 7.4, t 37 ºC); symbols stand for experimental data; lines represent the fitted curves; Experimental conditions: oxidation potential, 3.0 V; oxidation time, 120 min; electrolyte, 1M CH_3COOH or 1M H_2SO_4 solutions.

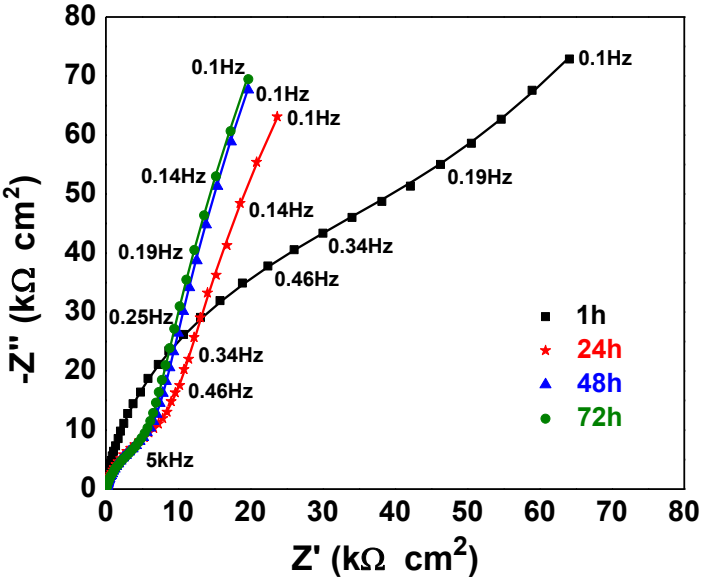

Figure 4.11 Nyquist plots for the corrosion of Ti–6Al–7Nb samples recorded at different exposure times after immersion in Hank's physiological solution (pH 7.4, t 37 ºC). Experimental conditions: oxidation potential, 3.0 V; oxidation time, 120 min; electrolyte, 1M CH_3COOH solution.

Table 4.4 Values of fitted parameters of the equivalent 2RC circuit of untreated and anodically oxidized Ti–6Al–7Nb alloy immersed in simulated physiological solution.

R_e (Ω cm^2)	R_p (kΩ cm^2)	Q_p ($\mu\Omega^{-1}$ s^n cm^{-2})	n_1	C_p (μF cm^{-2})	R_b (MΩ cm^2)	Q_b ($\mu\Omega^{-1}$ s^n cm^{-2})	n_2	C_b (μF cm^{-2})
untreated sample (1 h immersion)								
32.11	0.75	14.03	0.986	14.51	0.93	15.71	0.879	22.72
oxidized at 3.0 V in CH_3COOH (1 h immersion)								
26.64	8.65	6.38	0.939	8.27	16.45	0.19	0.903	0.21
oxidized at 3.0 V in CH_3COOH (72 h immersion)								
28.86	0.48	4.29	0.883	4.72	105.79	2.36	0.948	3.19
oxidized at 3.0 V in H_2SO_4 (1 h immersion)								
24.37	3.12	5.81	0.901	7.98	12.94	0.11	0.875	0.12
oxidized at 3.0 V in H_2SO_4 (72 h immersion)								
25.96	1.02	4.71	0.897	5.64	98.37	2.33	0.939	3.31

4.3. Ag-TiO_2 composite layer with improved corrosion and antimicrobial properties deposited on Ti by sol-gel method

4.3.3.1. Phase composition, microstructure, optical properties and morphology of the coatings

Phase composition and microstructure of the coatings were obtained by XRD analysis. The powdered samples were obtained by drying TiO_2 and Ag-TiO_2 sols for 12 hours at 100 °C, a temperature just sufficient for the removal of the liquid solvent. XRD spectra of samples are shown in Figure 4.13.

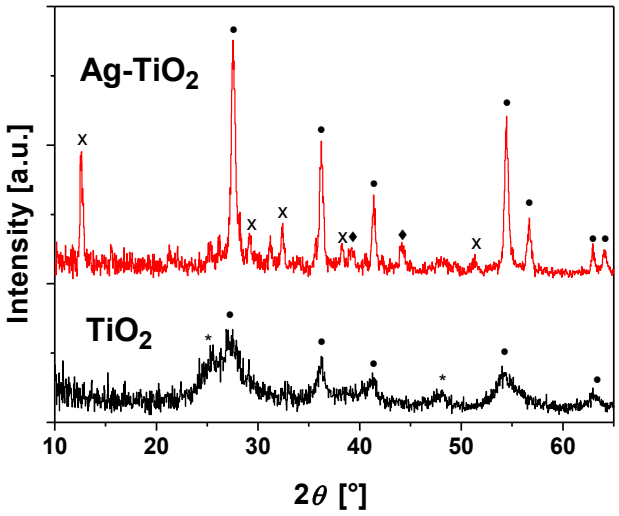

Figure 4.13 XRD spectra for TiO_2 and Ag-TiO_2 powders obtained by drying TiO_2 and Ag-TiO_2 sols for 12 hours at 100 °C. Diffraction peaks of (●) rutile, (*) anatase, (♦) silver and (x) ammonium silver nitrate.

The morphology and composition of the coated titanium samples were analysed by SEM-EDS analysis. The TiO_2 coating is homogeneous with occasional pinholes (Figure 4.15(a)). The grinding marks are still visible below the coating indicating that its thickness probably does not exceed 100-200 nm.

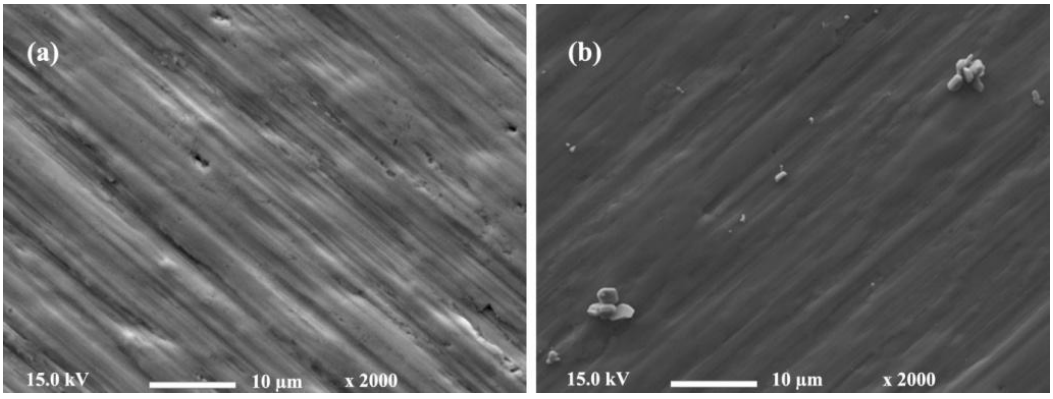

Figure 4.15 SEM images of (a) TiO_2 and (b) Ag-TiO_2 coatings on titanium substrate. EDS spectrum taken at the particle confirms the presence of silver (Figure 4.16(b)).

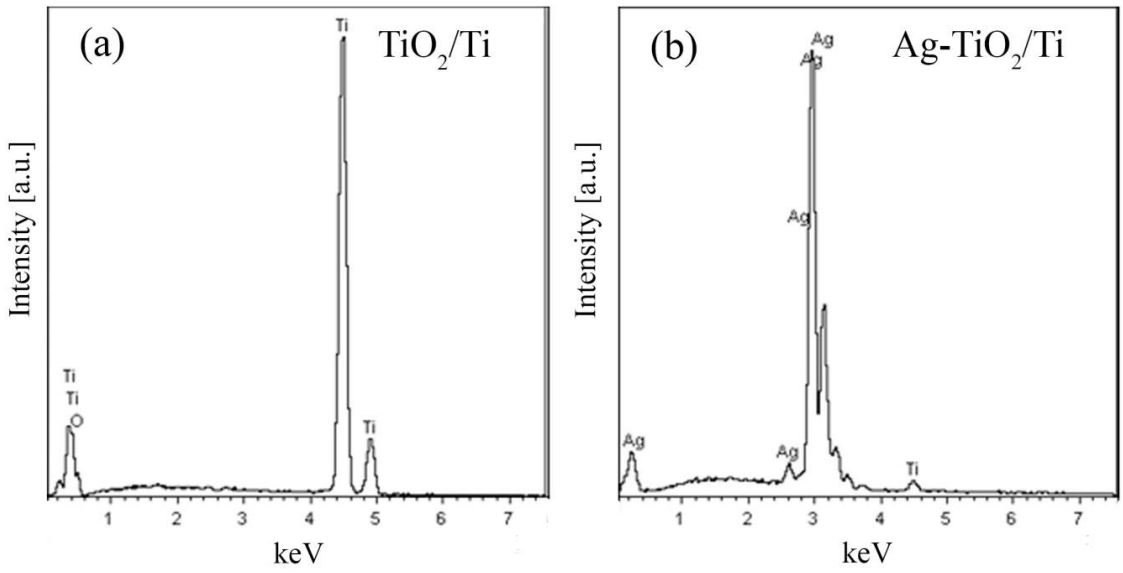

Figure 4.16 EDS analysis of (a) TiO_2 and (b) Ag-TiO_2 coatings on titanium substrate. Spectrum (a) was taken at the TiO_2 coatings and (b) at the silver nanoparticles.

4.3.3.2. Electrochemical characteristics of the coatings

4.3.3.2.1. Polarization resistance and potentiodynamic curves

Potentiodynamic polarization curves recorded of uncoated Ti and Ag samples, and Ti coated with TiO_2 and different Ag-TiO_2 coatings are presented in Figure 4.17 after 1 h and 120 h immersion in Hank's solution, *e.g.*, after EIS measurements. The deduced corrosion parameters: E_{oc}, R_p, E_{corr}, i_{corr} and Tafel slopes (b_a and b_c), are presented in Table 4.5.

After the stabilization at the E_{oc} the values of polarization resistance in SBF are approximately 10 times larger for Ti than for Ag indicating higher corrosion resistance (Table 4.5). The polarization curve for Ti also reflects its high corrosion resistance in this environment (Figure 4.17). Following the Tafel region, a broad passive range is established extending from 0.5 V to high anodic potentials of almost 8.0 V (presented up to 2.0 V in Figure 4.17).

Table 4.5 Corrosion parameters measured in simulated body fluid, pH 7.4, t 37 ºC, for uncoated Ti and Ag, and Ti samples coated with TiO_2 and Ag-TiO_2 coatings. The corrosion parameters were measured after 1 h immersion and after 120 h immersion, *e.g.*, after EIS measurements.

Sample	E_{oc} **(mV *vs.* Ag/AgCl,KCl$_{3M}$)**	R_p **(kΩ cm^2)**	E_{corr} **(mV *vs.* Ag/AgCl,KCl$_{3M}$)**	i_{corr} **(nA cm^{-2})**	b_a **(mV/decade)**	b_c **(mV/decade)**
Uncoated samples						
Ti	-220	236	-226	101	89	211
Ag	-68	27	-73	237	50	36
Coated samples after 1 h immersion						
TiO_2/Ti	82	198	54	79	97	97
Ag-TiO_2/Ti	7	602	-21	15	87	62
Coated samples after 120 h immersion						
TiO_2/Ti	83	1145	-40	4	85	276
Ag-TiO_2/Ti	75	1109	-44	4	95	329

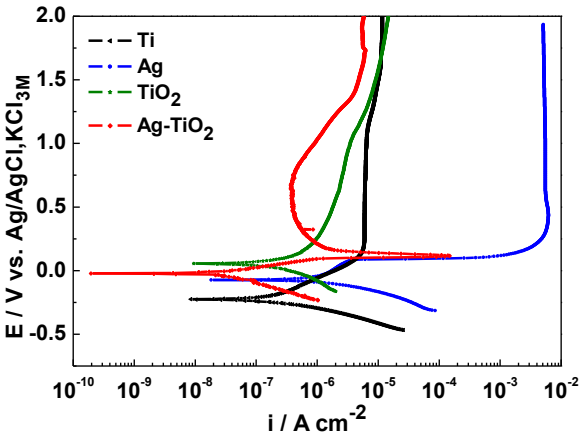

Figure 4.17 Potentiodynamic polarization curves recorded in simulated body fluid at 37 °C for uncoated Ti and Ag substrates, and Ti substrates coated with TiO_2 and Ag-TiO_2 coatings after 1 h immersion at the $E_{oc.}$

4.3.3.2.2. Electrochemical impedance spectroscopy

Some information about the mechanism of corrosion protection by deposited coatings and to investigate how they are affected by the immersion in SBF are provided by EIS measurements. The results are presented in the form of Nyquist plots (Figure 4. 18).

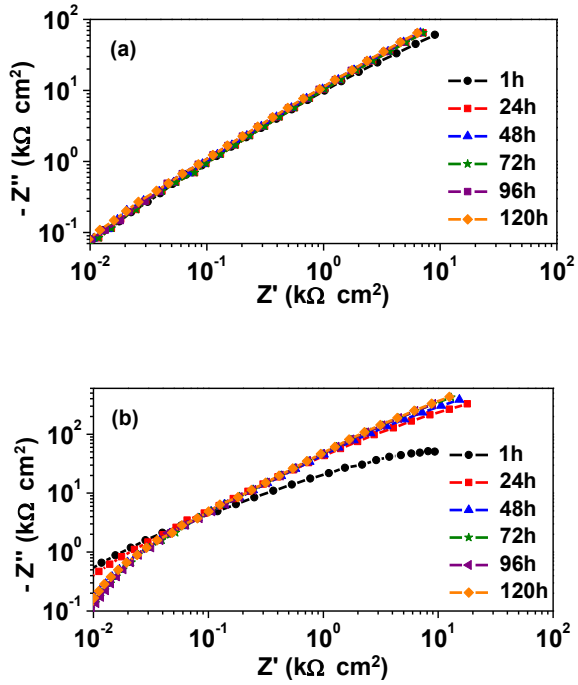

Figure 4.18 Nyquist plots for Ti coated with TiO_2 (a) and Ag-TiO_2 (b) coatings at different immersion times in simulated body fluid, pH 7.4 at t 37 ºC.

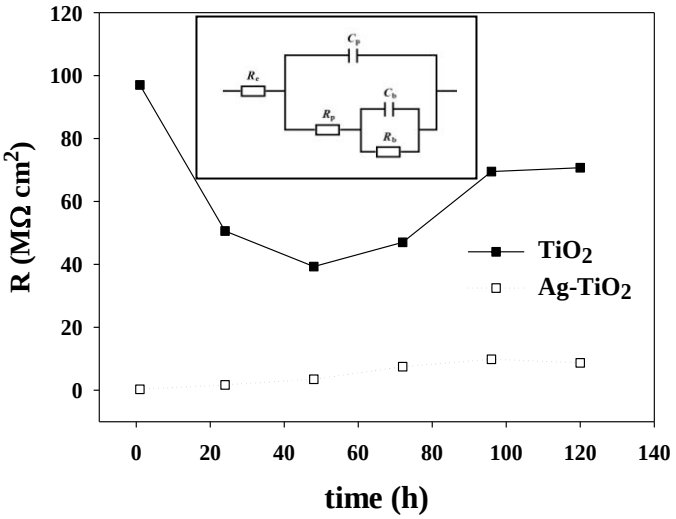

Figure 4.21 Evolution of total resistance presented as the sum of partial resistance as a function of time immersion in simulated body fluid. Electrical equivalent circuit used for interpreting the experimental impedance data (Inset).

The electrical equivalent circuit presented in Figure 4.21 (Inset) is based on a two layer structure of the passive film (a dense inner layer and a porous outer layer). It assumes that the barrier layer is compact and manifests a very large resistance, whereas the outer layer contains micropores [60].

In this equivalent circuit, R_e is the solution resistance, the parameters R_p and C_p describe the reactions of the outer porous passive film/solution interface, and the parameters R_b and C_b are attributed to the processes at the inner barrier layer at the electrolyte/passive film interface. C_b and C_p, the elements represented in both circuits as capacitors, were fitted as constant phase elements (CPEs) represented by the terms Q and n. The impedance of CPE is given by equation (4.2) [147] where j is an imaginary number ($\sqrt{-1}$) and ω is the angular frequency in rad s^{-1}; depending on the value of the exponent n, CPE could be a resistor with resistance R (n = 0); a capacitor with capacitance C (n = 1); a Warburg impedance, W (n = 0.5) or an inductance, L (n = -1). The values of n are associated with non-uniform distribution of current as a result of roughness and surface defects.

$$Q = Z_{CPE(\omega)} = [C(j\omega)^n]^{-1} \quad (4.2)$$

The values of the equivalent circuit component obtained by adjusting the experimental data, using the equivalent circuit illustrated in Figure 4.21 (Inset), are shown in Table 4.6.

Table 4.6 Values of fitted parameters of the equivalent circuit as a function of the immersion time of TiO_2 and Ag-TiO_2 coated Ti in simulated body fluid. Please note the difference in units for R_b and R_p.

Time (h)	Re (Ω cm^2)	R_p (Ω cm^2)	Q_p ($\mu\Omega^{-1}$ s^n m^{-2})	n_1	C_p (μF cm^{-2})	R_b (MΩ cm^2)	Q_b ($\mu\Omega^{-1}$ s^n m^{-2})	n_2	C_b (μF cm^{-2})
TiO_2/Ti									
1	26	9.8	0.17	0.997	0.16	97.0	18.2	0.898	42.7
24	26	8.4	1.95	0.826	/	50.6	14.8	0.925	25.3
48	22	11.7	0.22	0.961	0.06	39.3	16.1	0.918	28.5
72	20	13.5	0.21	0.934	0.02	47.0	16.2	0.918	29.2
96	21	13.0	2.37	0.928	0.02	69.5	16.1	0.919	29.8
120	22	11.4	0.11	1.000	0.10	70.7	16.3	0.919	30.3
Ag-TiO_2/Ti									
1	32	62.3	19.90	0.935	12.5	0.3	10.3	0.884	11.8
24	34	57.3	8.49	0.950	5.7	1.7	12.2	0.817	24.1
48	36	138.3	10.40	0.837	2.9	3.5	9.6	0.898	14.3
72	42	154.8	9.34	0.838	2.6	7.5	10.2	0.896	16.8
96	44	152.1	9.69	0.831	2.6	9.8	9.9	0.902	16.3
120	41	112.8	9.24	0.843	2.6	8.7	10.3	0.898	17.1

4.3.3.3. Topography of the coatings

In order to determine the topography and surface roughness 3D-profilometry profiles were recorded for TiO_2 and Ag-TiO_2 before and after electrochemical tests (potentiodynamic curves (PD)) presented in Figure 4.22.

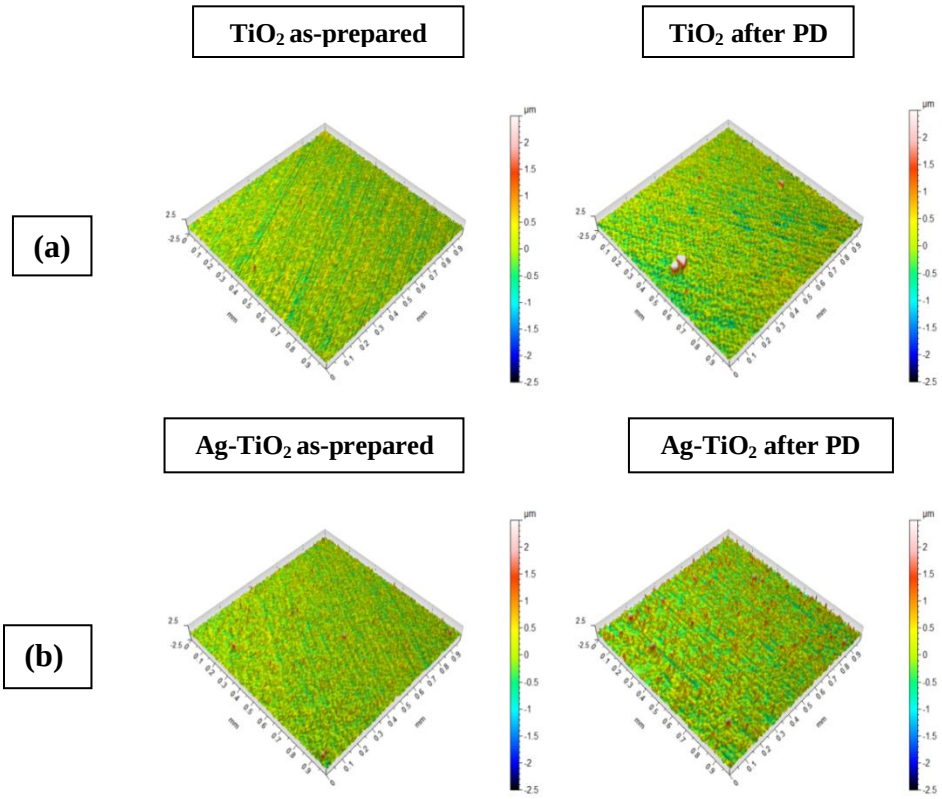

Figure 4.22 Side view of profiles of (a) TiO_2 and (b) Ag-TiO_2 coated titanium substrates recorded for: (a) as prepared coatings cured 1 h at 150 °C, (b) after potentiodynamic measurements in simulated body fluid (Figure 4.17).

4.3.3.4. Adhesion of bacteria to the coatings

In order to investigate the antibacterial properties of the synthesized coatings the adhesion and morphology of adhered bacteria *Pseudomonas aeruginosa* were analyzed. The adhesion of bacteria to the coating surface was expressed as relative fluorescence generated from bacteria attached to TiO_2 and Ag-TiO_2 coated samples to bacteria attached to uncoated Ti sample (Figure 4.23). The adhesion of bacteria to coated surface was smaller than to the uncoated surface; however, the difference was not statistically significant.

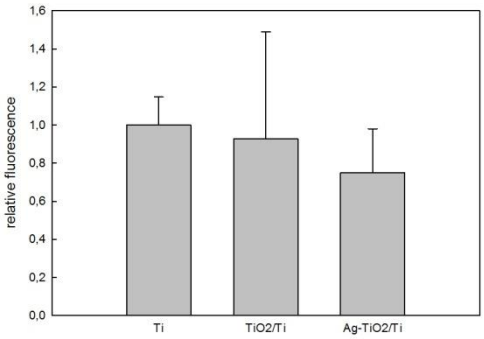

Figure 4.23 Adhesion of *Pseudomonas aeruginosa* on uncoated Ti and Ti coated with TiO_2 and Ag-TiO_2 coatings. Samples were incubated with $1x10^8$ CFU/mL bacteria overnight at 37 °C.

After the test, the morphology of bacteria was imaged by SEM (Figure 4.24). SEM images show that the number of bacteria present is similar for uncoated Ti and Ti coated with TiO_2; however, for Ag-TiO_2 coating the bacteria seem to be less numerous.

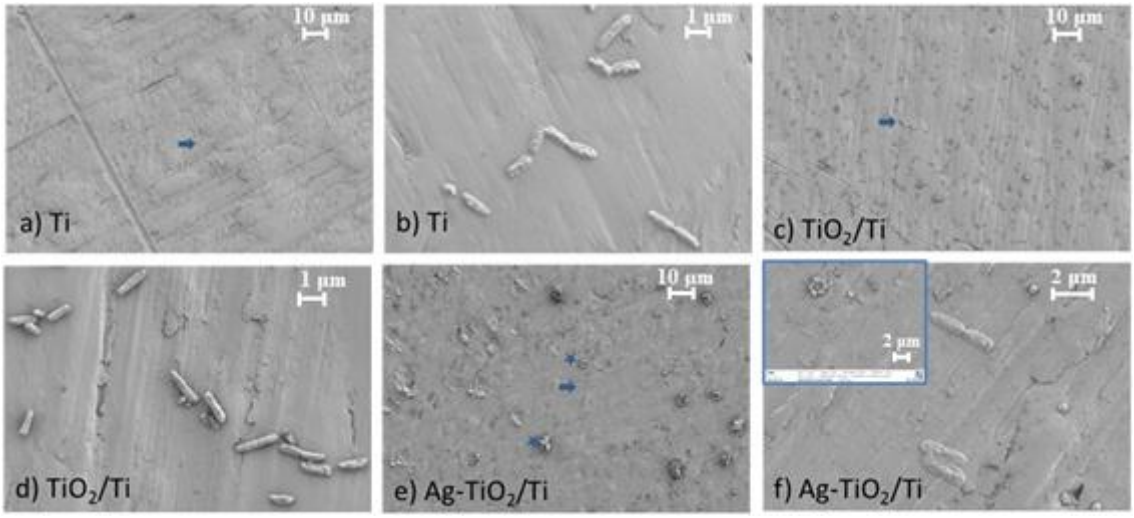

Figure 4.24 SEM images of bacteria *Pseudomonas aeruginosa* adhered to the surface of uncoated Ti and Ti coated with TiO_2 and Ag-TiO_2 coatings. Samples were incubated with $1x10^8$ CFU/mL bacteria overnight at 37 °C. After testing, the samples were prepared for imaging as described in Experimental. Magnifications (a,c,e) 1,000×, and (b,d,f) 20,000×. Inset in (f) shows agglomerated Ag nanoparticles. (a,c,e) Arrow points to bacteria and stars to agglomerated Ag particles.

5. Corrosion resistant coatings for galvanized steel

5.3.1. Preliminary measurements on sol-gel coated Zn substrates

Before studying the behavior of silica coatings on galvanized steel substrates, some electrochemical experiments were carried out with the coatings deposited on Zn wafers.

5.3.1.1. Electrochemical measurements

5.3.1.1.1. Polarization curves

Polarization curves were recorded at constant sweep rate of 10 mV min^{-1} in a potential range of ± 200 mV *vs.* open circuit potential. Figure 5.3 show representative Tafel polarization curves for Zn and of different silica-coated Zn samples immersed in 0.2 g L^{-1} Na_2SO_4 (pH 5.0) solution at 25 ºC. The values of the open circuit potential are situated around -1 V *vs.* Ag/AgCl,$NaCl_{3M}$ with very small variations.

The electrochemical parameters, such as the corrosion potential (E_{corr}) and the corrosion current density (i_{corr}) were estimated by extrapolation of the Tafel lines. The resulted values for all type of samples are collected in Table 5.3.

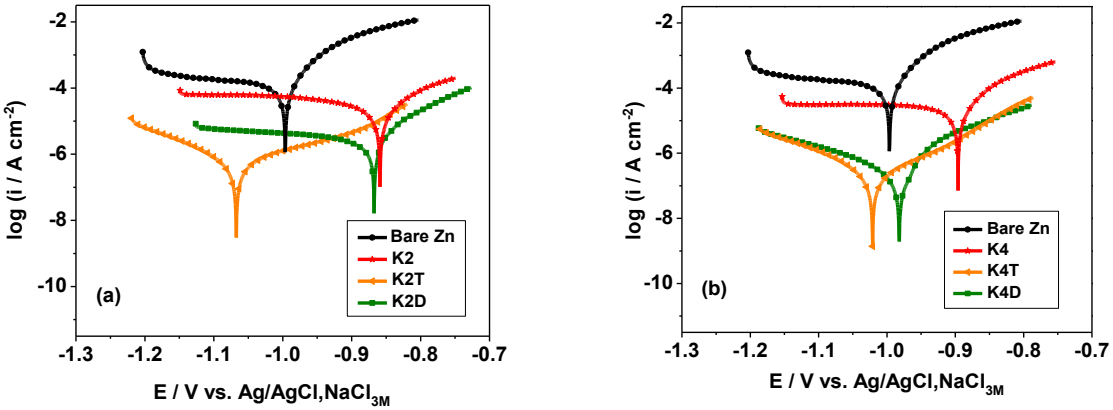

Figure 5.3 Polarization curves obtained for the bare Zn substrate and for Zn covered with silica layers: (a) double-dipped compact (K2) and (b) four–dipped compact (K4) silylated with TMClSi (T) or DMDClSi (D).

Moreover, the CTAB–templated without TMClSi or DMDClSi (untreated or unsilanized) coating shows better anti–corrosion behavior than the unsilanized compact or Pluronic–type double–dipped samples (Table 5.3). The latter finding is quite expectable taking into consideration the difficult accessibility of the pore system of the CTAB–type samples as was already reported [86].

Table 5.3 Kinetic parameters of the corrosion process obtained by regression using the Tafel interpretation of the polarization curves (E_{corr} is corrosion potential, i_{corr} is corrosion current density, E_{oc} is open circuit potential, *P.E.* is protection efficiency).

Sample	E_{corr} [V *vs.* Ag/AgCl,$NaCl_{3M}$]	i_{corr} [µA cm^{-2}]	E_{oc} [V *vs.* Ag/AgCl,$NaCl_{3M}$]	*P.E.* [%]
Bare *Zn*	-0.996	12.15 ± 0.912	-0.962	-
K2	-0.859	6.427 ± 0.993	-1.020	47.16
K2T	-1.026	0.302 ± 0.014	-1.003	97.51
K2D	-0.867	0.525 ± 0.107	-1.021	95.67
K4	-0.896	1.650 ± 0.220	-1.012	86.41
K4T	-1.021	0.063 ± 0.012	-0.986	99.48
K4D	-0.982	0.039 ± 0.009	-0.998	**99.67**
C2	-0.864	3.020 ± 0.902	-0.967	75.14
C2T	-1.09	0.329 ± 0.120	-1.033	97.29
C2D	-0.949	0.122 ± 0.024	-0.996	98.99
P2	-0.915	6.107 ± 0.608	-1.006	49.73
P2T	-1.061	0.269 ± 0.029	-0.949	97.78
P2D	-1.072	0.202 ± 0.069	-0.983	98.33

5.3.1.1.2. Electrochemical impedance spectroscopy

Figure 5.6 shows the impedance spectra recorded for different coated samples after 1 hour of immersion in the corrosive environment (0.2 g L^{-1} Na_2SO_4, pH 5.0).

The diagrams show a capacitive behavior and a large value of the polarization resistance that suggests a corrosion resistive interface.

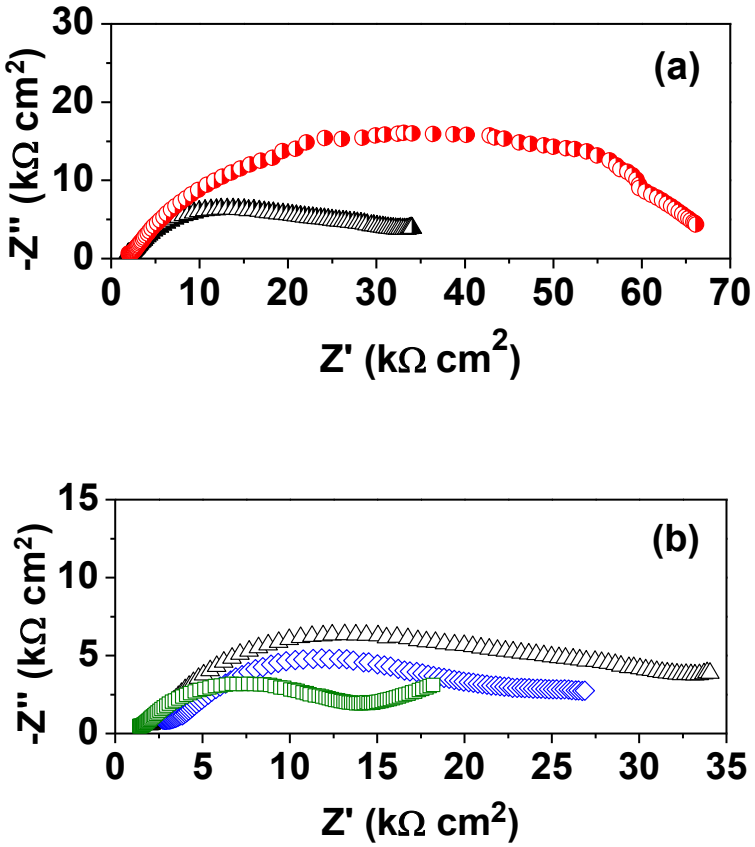

Figure 5.6 Impedance Nyquist plots recorded at E_{oc} of silica-coated Zn in 0.2 g L^{-1} Na_2SO_4 (pH 5.0): (a) double–dipped compact (K2T) (*empty triangle*) *vs.* four–dipped compact (K4T) (*empty circle*) sample and (b) double–dipped compact (K2T) (*empty triangle*) *vs.* Pluronic–templated porous (P2T) (*empty rhomb*) *vs.* CTAB–templated porous coating annealed after each dipping step (C2HT) (*empty square*). All the presented samples were silylated with TMClSi (T).

The values of the equivalent circuit component were obtained adjusting the experimental data which are shown in Table 5.4. In this equivalent circuit, R_e is the solution resistance, the parameters R_p and C_p describe the reactions of the outer porous passive film/interface, and the parameters R_b and C_b are attributed to the processes at the inner barrier layer at the electrolyte/passive film interface.

Impedance diagrams, in good agreement with Tafel plots, show that four-layer coatings (K4T) ensure higher protection against corrosion than the same type double-layer coatings (K2T) see Figure 5.6(a)). Furthermore, as also stated at the interpretation of Tafel plots, it can be seen that the effect of pore structure and thermal treatment on the corrosion resistance is not remarkable (Figure 5.6(b)).

Table 5.4 Values of fitted parameters of the equivalent circuit of silica-coated Zn samples in 0.2 g L^{-1} Na_2SO_4 (pH 5.0): double–dipped compact; four–dipped compact (K4T); Pluronic–templated porous (P2T) and CTAB–templated porous coating annealed after each dipping step (C2HT). All the presented samples were silylated with TMClSi (T).

Sample	R_e (kΩ cm^2)	R_p (kΩ cm^2)	Q_p (μ$Ω^{-1}$ s^n m^{-2})	n_1	C_p (μF cm^{-2})	R_b (kΩ cm^2)	Q_b (μ$Ω^{-1}$ s^n m^{-2})	n_2	C_b (μF cm^{-2})
K2T	0.9	3.98	5.17	0.621	0.48	35.98	0.05	0.856	0.02
K4T	1.4	3.45	1.22	0.519	0.07	65.33	0.03	0.895	0.01
P2T	2.4	7.86	6.52	0.574	0.72	23.48	0.05	0.884	0.02
C2HT	0.6	6.40	2.67	0.576	0.13	10.27	33	0.667	62

5.3.2. Silica coatings on galvanized steel

5.3.2.1. Characterization of the samples by SEM measurements

SEM analysis of the non-silylated SiO_2/CTAB porous samples dipped in BTA solution for 30 minutes (Figure 5.10) reveals that a more uniform surface can be observed in the case of electrolytically Zn coated substrates than in the case of hot-dip Zn coated steel.

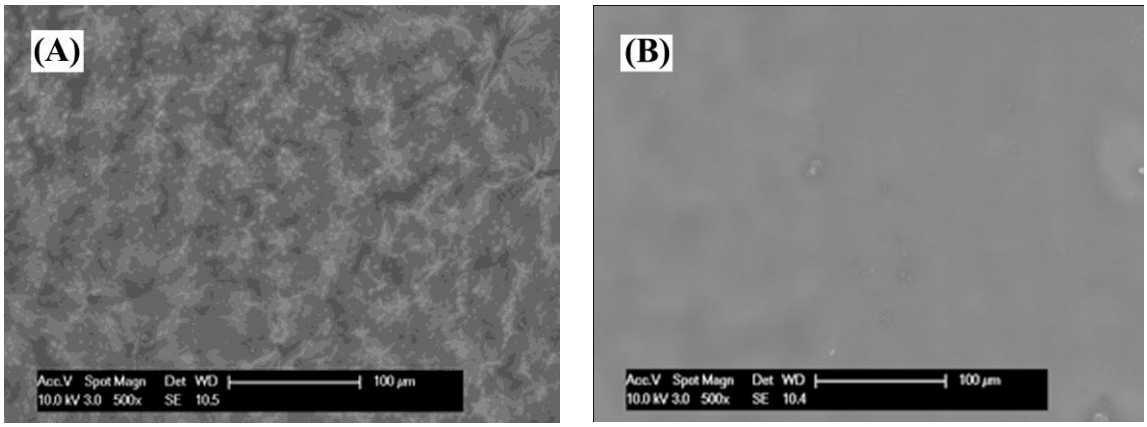

Figure 5.10 SEM micrographs of BTA impregnated CTAB/SiO_2 porous bilayers deposited on hot-dip (A) and electrolytic (B) zinc coatings on steel.

5.3.2.2. HRTEM analysis of the pore structure

Transmission electron microscope images taken on the monolayered Pluronic- and CTAB-templated SiO_2 samples prepared onto Si substrates support this idea (Figure 5.11). Thus, CTAB-templated SiO_2 samples exhibit smaller pores than Pluronic templated samples.

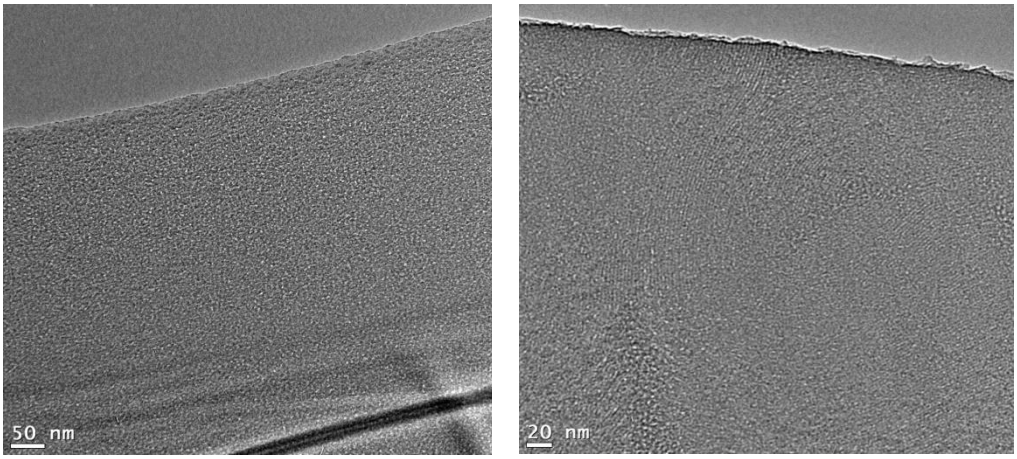

Figure 5.11 HRTEM images taken on the monolayered Pluronic- and CTAB-templated SiO_2 samples prepared onto Si substrates.

5.3.2.3. Electrochemical measurements

5.3.2.3.1. Polarization curves

The Tafel polarization curves of compact silica coated (silylated and non-silylated) samples are presented in Figure 5.12. Corrosion tests were carried out in 0.2 g L^{-1} aqueous solution of Na_2SO_4 (pH 5.0).

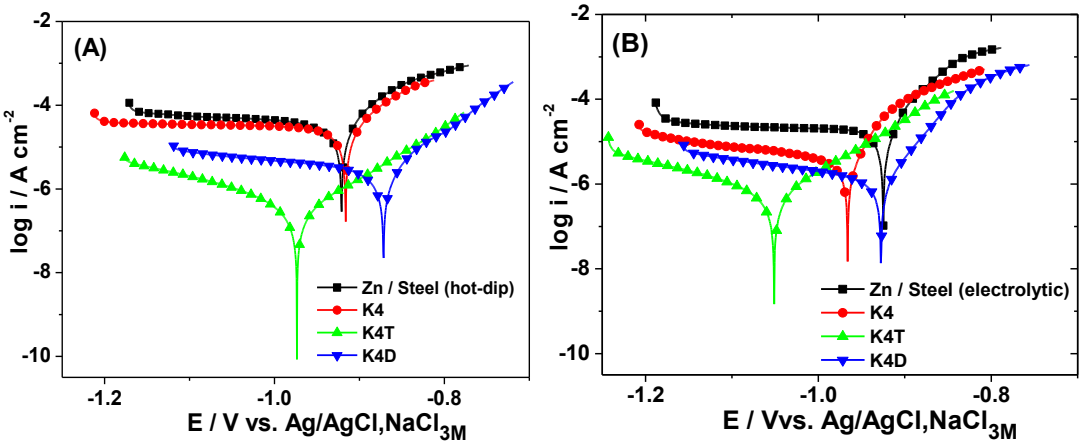

Figure 5.12 Tafel curves obtained for the compact silica coatings. T: TMClSi; D: DMDClSi; K4: compact, four layered SiO_2 coatings deposited on hot-dip (A) and on electrolytic (B) zinc coatings on steel.

The experimentally obtained electrochemical parameters which can characterize the corrosion process are presented in Table 5.5 for the investigated samples.

Table 5.5 Results of electrochemical measurements on zinc plated steel covered with compact and porous sol-gel silica coatings.

Sample	i_{corr} [μA cm^{-2}]	E_{corr} [V *vs.* Ag/AgCl]	b_c [V/decade]	b_a [V/decade]	i_{corr} [μA cm^{-2}]	E_{corr} [V *vs.* Ag/AgCl]	b_c [V/decade]	b_a [V/decade]
	Hot-dip zinc coating				**Electrolytic zinc coating**			
***Zn* / Steel**	5.946 ± 0.560	-0.921	0.074	0.033	3.530 ± 0.490	-0.925	0.066	0.028
C2	3.559 ± 0.600	-0.910	0.144	0.048	1.649 ± 0.050	-0.920	0.073	0.026
C2T	0.398 ± 0.001	-1.031	0.119	0.085	0.161 ± 0.019	-1.037	0.055	0.060
C2D	0.199 ± 0.001	-0.982	0.102	0.105	0.074 ± 0.012	-0.980	0.071	0.070
K4	3.130 ± 0.001	-0.916	0.040	0.024	0.850 ± 0.173	-0.966	0.073	0.027
K4T	0.090 ± 0.004	-0.974	0.092	0.073	0.125 ± 0.007	-1.018	0.058	0.101
K4D	0.667 ± 0.012	-0.872	0.132	0.049	0.054 ± 0.001	-0.928	0.094	0.035

5.3.2.3.2. Electrochemical impedance spectroscopy

For a better understanding of the protection mechanism involving the silica layers, Nyquist and Bode plots of the porous and compact sol-gel silica coatings deposited on hot-dip Zn coatings on steel, were recorded in the absence and in the presence of the silylating agents and are presented in Figure 5.17.

The values of each element in the equivalent circuits were calculated using ZSimpWin 3.21 software. The used equivalent circuits provide adequate fitting of all experimental results as can be seen in Table 5.17.

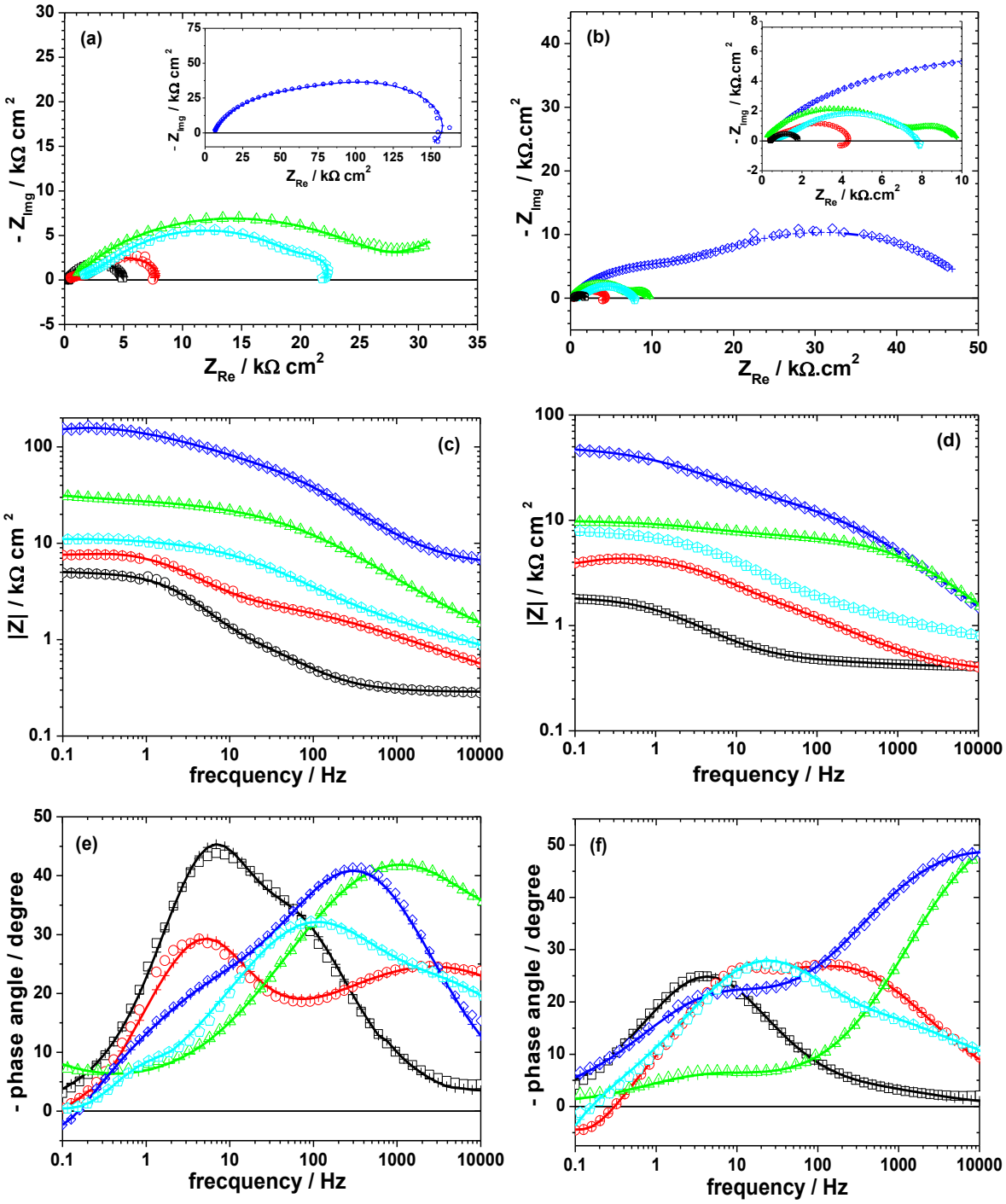

Figure 5.17 Nyquist (a, b) and Bode (c, d, e, f) impedance spectra of CTAB/porous SiO_2 layers deposited on electrolytic (left) and hot-dip (right) zinc coatings on steel . (□) Zn/steel; (○) C2; (Δ) C2T; (◊) C2D; (⌂) C2-BTA 30 min. The symbols correspond to the experimental data and the line with cross (—+—) to the calculated data.

Table 5.7 Electrical elements fitted values for the hot-dip zinc plated steel covered with porous (C) and compact (K) sol-gel silica coatings.

Sample	R_e (kΩ cm^2)	R_{coat} (kΩ cm^2)	Q_{coat} (μF s^{n-1} cm^{-2})	n_1	R_{ct} (kΩ cm^2)	Q_{dl} (μF s^{n-1} cm^{-2})	n_2	χ^2
***Zn* / Steel (hot-dip)**	0.40 ± 0.58	0.08 ± 12.65	40.67 ± 14.66	0.71	1.43 ± 1.25	97.30 ± 6.41	0.72	$1.19\ 10^{-4}$
C2	0.32 ± 0.69	1.93 ± 3.37	19.94 ± 1.31	0.56	2.43 ± 3.43	12.78 ± 8.35	0.81	$4.16\ 10^{-5}$
C2T	0.09 ± 19.78	7.10 ± 0.73	0.29 ± 3.64	0.69	2.77 ± 2.30	52.45 ± 3.75	0.64	$5.11\ 10^{-5}$
C2D	0.10 ± 25.63	17.12 ± 2.65	0.73 ± 5.78	0.62	33.64 ± 2.01	6.33 ± 2.40	0.62	$8.85\ 10^{-5}$
***C2 BTA* 30min**	0.64 ± 1.45	1.31 ± 5.64	8.26 ± 4.51	0.56	6.22 ± 1.56	9.30 ± 5.50	0.68	$2.01\ 10^{-4}$
K4	0.41 ± 4.40	0.45 ± 2.49	19.75·± 14.09	0.52	2.20 ± 2.12	98.85 ± 5.05	0.74	$5.67\ 10^{-4}$
K4T	0.28 (n.d)	44.38 ± 3.31	0.52 ± 3.30	0.61	41.60 ± 4.39	4.37 ± 3.87	0.65	$1.36\ 10^{-4}$
K4D	0.71 ± 7.53	23.02 ± 3.63	0.65 ± 1.73	0.68	30.04 ± 6.18	14.07 ± 12.50	0.51	$2.52\ 10^{-3}$

CONCLUSIONS

✓ Sol-gel TiO_2 and Ag-TiO_2 coatings were synthesized and deposited on titanium substrate by spin-coating in order to increase the functionality of the surface for biomedical applications. The addition of $AgNO_3$ to synthesis route results in the formation of Ag-TiO_2. The silver particles shift the absorption of TiO_2 to the visible region, as shown by UV-Vis spectroscopy. Electrochemical polarization measurements of deposited coatings in simulated physiological solution confirm their protective properties which are reflected in increased polarization resistance and decrease in corrosion current density compared to uncoated titanium. Antibacterial properties of deposited coatings were investigated in the presence of *Pseudomonas aeruginosa*, a biofilm forming bacteria. The adhesion of bacteria is reduced on coated titanium in comparison to uncoated substrate.

✓ TiO_2 layers were obtained on the surface of Ti-6Al-7Nb substrate by anodic oxidation in acetic and sulfuric acids. The formation of TiO_2 on the Ti–6Al–7Nb substrate beneficially affects its corrosion behavior in simulated physiological solution. The samples oxidized in CH_3COOH present on their surface a thicker oxide layer compared with the oxide layer formed on H_2SO_4 surface. The most intense diffraction peak belonging to rutile, but anatase is also present. The oxidation in CH_3COOH seems to be more beneficial for the corrosion resistance of Ti–6Al–7Nb samples than the oxidation in H_2SO_4 of same concentration leading to smaller corrosion current density values.

✓ Thin (mesoporous and compact) silica coatings were prepared on Zn substrates for the preliminary electrochemical examinations. The corrosion resistance of any coated investigated samples was significantly better than that of the bare Zn substrate. Rendering the coatings hydrophobic by two types of silylating agents (DMDClSi and TMClSi) the corrosion current density for both the porous and compact coatings diminished with one or even two orders of magnitude.

✓ In case of silica coatings deposited on galvanized steel substrate the layers deposited on electrolytically coated steel confer generally better protection than those deposited on hot-dip

coated steel, due to the fact that the electrolytic Zn coatings are more uniform than the hot-dip ones and, consequently, the silica layers deposited on their top are too. The hydrophobic silica coatings presented in this work improve the corrosion resistance of Zn-coated steel. The best improvement in the case of CTAB-silica porous layers was obtained when silylation was carried out by using DMDClSi, while in the case of compact silica layers on hot-dip Zn coatings, TMClSi has a better effect than DMDClSi.

SCIENTIFIC ACTIVITY

Papers

1. Patrick Ioan Nemes, **Nicoleta Cotolan**, Liana Maria Mureşan, Corrosion Behaviour of Composite Coatings Obtained by Electrolytic Codeposition of Zinc with Nanoparticles of $CeO_2 \cdot ZrO_2$ Binary Oxides, *Studia Universitatis Babeş-Bolyai, Chemia*, 58 (LVIII), **2013,** 81–93. (IF=0.136)

2. Nicoleta Cotolan, Aurel Pop, Daniel Marconi, Oana Ponta, Liana Maria Mureşan, Corrosion Behavior of Titanium Dioxide-coated Ti−6Al−7Nb Surfaces Obtained by Anodic Oxidation in Sulfuric or Acetic Acid, *Materials and Corrrosion*, 66, **2015**, 635–642. (IF=1.508)

3. Emoke Albert, **Nicoleta Cotolan**, Norbert Nagy, György Sáfrán, Gabriella Szabó, Liana-Maria Mureşan, Zoltán Hórvölgyi, Mesoporous silica coatings with improved corrosion protection properties, *Microporous and Mesoporous Materials*, 206, **2015,** 102–113. (IF=3.453)

4. Nicoleta Cotolan, Simona Varvara, Emőke Albert, Gabriella Szabó, Zoltán Hórvölgyi, Liana-Maria Mureşan, Evaluation of corrosion inhibition performance of silica sol-gel layers deposited on galvanised steel, *Corrosion Engineering Science and Technology* accepted. (IF=0.831)

5. Nicoleta Cotolan, Mitja Rak, Marjan Bele, Andrej Cör, Liana-Maria Mureşan, Ingrid Milošev, Synthesis of Ag-TiO_2 coatings on titanium substrate by sol-gel method and their characterization, submitted to *Materials Science and Engineering C*. (IF=3.088)

Conferences participation

1. Nicoleta Cotolan, Emőke Albert, Erika Nagy, Zoltán Hórvölgyi, Gabriella Szabó, Liana-Maria Mureşan, Corrosion behaviour of silica coated Zn substrates: the role of thickness and thermal treatment of protective layers, *19th International Conference on Chemistry*, Baia-Mare, Romania, **2013** November **(poster presentation)**.

2. Albert Emőke, **Nicoleta Cotolan**, Nagy Erika, Hórvölgyi Zoltán, Szabó Gabriella, Liana-Maria Mureşan, The effect of modified silica coatings on the corrosion behaviour of Zn substrates: the role of silylating and templating agents, *19th International Conference on Chemistry*, Baia-Mare, Romania, **2013** November **(poster presentation)**.

3. Nicoleta Cotolan, Liana Maria Mureşan, Corrosion studies of Ag-TiO_2–coated Ti−6Al−7Nb surfaces in simulated physiological solution, *4th Regional Symposium on Electrochemistry South-East Europe (RSE-SEE)*, Ljubljana, Slovenia, **2013** May **(poster presentation)**.

4. Nicoleta Cotolan, Aurel Pop, Daniel Marconi, Oana Ponta, Liana Maria Mureşan, TiO_2–coated Ti–6Al–7Nb surfaces obtained by anodic oxidation - study of the corrosion behavior, *5th Conference on Advanced Spectroscopies on Biomedical and Nanostructured Systems*, Cluj-Napoca, Romania, **2014** September **(poster presentation)**.

5. Nicoleta Cotolan, Emőke Albert, Gabriella Szabó, Zoltán Hórvölgyi, Liana-Maria Mureşan, Improvement in the oxidation resistance of zinc coated steel substrates by sol-gel derived silica film, *20th International Conference on Chemistry*, Cluj-Napoca, Romania, **2014** November **(poster presentation)**.

6. Nicoleta Cotolan, Liana-Maria Mureşan, Marjan Bele and Ingrid Milošev, Synthesis of Ag-TiO_2 coatings on titanium substrate by sol-gel method and their characterization, *5th Regional Symposium on Electrochemistry South-East Europe (RSE–SEE)*, Pravets, Bulgaria, **2015** June **(oral presentation)**. Awarded for the Best Young Oral Scientist Presentation.

SELECTED REFERENCES

1. Velten, D., et al., *Preparation of TiO_2 layers on cp–Ti and Ti6Al4V by thermal and anodic oxidation and by sol–gel coating techniques and their characterization.* Journal of Biomedical Materials Research, 2002. **59**: p. 18-28.
2. Okazaki, Y., *Effect of friction on anodic polarization properties of metallic biomaterials.* Biomaterials, 2002. **23**: p. 2071-2077.
3. Pan, J., D. Thierry, and C. Leygraf, *Electrochemical impedance spectroscopy study of the passive oxide film on titanium for implant application* Electrochimica Acta, 1996. **41**: p. 1143-1153.
4. Gonzalez, J.E.G. and J.C. Mirza-Rosca, *Study of the corrosion behavior of titanium and some of its alloys for biomedical and dental implant applications.* Journal of Electroanalytical Chemistry, 1999. **471**: p. 109-115.
5. Toumelin-Chemila, F., F. Rouellei, and G. Burdairon, *Corrosive properties of fluoride-containing odontologic gels against titanium.* Journal of Dentistry, 1996. **24**: p. 109-115.
6. Ochsenbein, A., et al., *Osteoblast responses to different oxide coatings produced by the sol-gel process on titanium substrates.* Acta Biomaterialia, 2008. **4**: p. 1506-1517.
7. Wang, K., H.W. Pickering, and K.G. Weil, *Corrosion Inhibition of Zinc by Benzotriazole with an Electrochemical Quartz Crystal Microbalance.* Journal of The Electrochemical Society, 2003. **150**: p. B176-B180.
8. Odnevall, I. and C. Leygraf, *Atmospheric Corrosion, ASTM STP 1239, (American Society for Testing and Materials)*. 1995, Philadelphia, PA.
9. Deslouis, C., M. Duprat, and C. Tournillon, *The kinetics of zinc dissolution in aerated sodium sulphate solutions. A measurement of the corrosion rate by impedance techniques.* Corrosion Science, 1989. **29**: p. 13-30.
60. Milošev, I., et al., *Effect of anodic oxidation on the corrosion behavior of Ti-based materials in simulated physiological solution.* Journal of Applied Electrochemistry, 2013. **43**: p. 645-658.
86. Albert, E., et al., *Mesoporous silica coatings with improved corrosion protection properties.* Microporous and Mesoporous Materials, 2015. **206**: p. 102-113.
147. Raistrick, I.D. and J. Macdonald, *Impedance Spectroscopy Theory, Experiment, and Applications*. A John Wiley & Sons. Vol. Second Edition. 1987, New Jersey: A John Wiley & Sons. 1-20.